Measurement of *CP* asymmetries in $B^0 \to \phi K_s^0$ decays with Belle II

I. Adachi, K. Adamczyk, L. Aggarwal, H. Ahmed, H. Aihara, N. Akopov, A. Aloisio, N. Anh Ky, D. M. Asner, H. Atmacan, T. Aushev, V. Aushev, M. Aversano, V. Babu, H. Bae, S. Bahinipati, P. Bambade, Sw. Banerjee, M. Barrett, J. Baudot, M. Bauer, A. Baur, A. Beaubien, F. Becherer, J. Becker, P. K. Behera, J. V. Bennett, V. Bertacchi, M. Bertemes, E. Bertholet, M. Bessner, S. Bettarini, B. Bhuyan, F. Bianchi, T. Bilka, D. Biswas, A. Bobrov, D. Bodrov, A. Bolz, A. Bondar, J. Borah, A. Bozek, M. Bračko, P. Branchini, R. A. Briere, T. E. Browder, A. Budano, S. Bussino, M. Campajola, L. Cao, G. Casarosa, C. Cecchi, J. Cerasoli, M.-C. Chang, P. Chang, P. Cheema, V. Chekelian, C. Chen, B. G. Cheon, K. Chilikin, K. Chirapatpimol, H.-E. Cho, K. Cho, S.-J. Cho, S.-K. Choi, S. Choudhury, J. Cochran, L. Corona, L. M. Cremaldi, S. Das, F. Dattola, E. De La Cruz-Burelo, S. A. De La Motte, G. De Nardo, M. De Nuccio, G. De Pietro, R. de Sangro, M. Destefanis, S. Dey, A. De Yta-Hernandez, R. Dhamija, A. Di Canto, F. Di Capua, J. Dingfelder, Z. Doležal, I. Domínguez Jiménez, T. V. Dong, M. Dorigo, K. Dort, S. Dreyer, S. Dubey, G. Dujany, P. Ecker, M. Eliachevitch, P. Feichtinger, T. Ferber, D. Ferlewicz, T. Fillinger, C. Finck, G. Finocchiaro, A. Fodor, F. Forti, A. Frey, B. G. Fulsom, A. Gabrielli, E. Ganiev, M. Garcia-Hernandez, A. Garmash, G. Gaudino, V. Gaur, A. Gaz, A. Gellrich, G. Ghevondyan, D. Ghosh, H. Ghumaryan, G. Giakoustidis, R. Giordano, A. Giri, A. Glazov, B. Gobbo, R. Godang, O. Gogota, P. Goldenzweig, W. Gradl, T. Grammatico, S. Granderath, E. Graziani, D. Greenwald, Z. Gruberová, T. Gu, Y. Guan, K. Gudkova, S. Halder, Y. Han, K. Hara, T. Hara, K. Hayasaka, H. Hayashii, S. Hazra, C. Hearty, M. T. Hedges, I. Heredia de la Cruz, M. Hernández Villanueva, A. Hershenhorn, T. Higuchi, E. C. Hill, M. Hoek, M. Hohmann, P. Horak, C.-L. Hsu, T. Humair, T. Iijima, K. Inami, N. Ipsita, A. Ishikawa, S. Ito, R. Itoh, M. Iwasaki, P. Jackson, W. W. Jacobs, E.-J. Jang, Q. P. Ji, S. Jia, Y. Jin, A. Johnson, K. K. Joo, H. Junkerkalefeld, A. B. Kaliyar, J. Kandra, K. H. Kang, S. Kang, G. Karyan, T. Kawasaki, F. Keil, C. Ketter, C. Kiesling, C.-H. Kim, D. Y. Kim, K.-H. Kim, Y.-K. Kim, H. Kindo, K. Kinoshita, P. Kodyš, T. Koga, S. Kohani, K. Kojima, T. Konno, A. Korobov, S. Korpar, E. Kovalenko, R. Kowalewski, T. M. G. Kraetzschmar, P. Križan, P. Krokovny, Y. Kulii, T. Kuhr, M. Kumar, K. Kumara, T. Kunigo, A. Kuzmin, Y.-J. Kwon, S. Lacaprara, Y.-T. Lai, T. Lam, L. Lanceri, J. S. Lange, M. Laurenza, K. Lautenbach, R. Leboucher, F. R. Le Diberder, M. J. Lee, P. Leitl, D. Levit, P. M. Lewis, C. Li, L. K. Li, J. Libby, Q. Y. Liu, Z. Q. Liu, D. Liventsev, S. Longo, A. Lozar, T. Lueck, C. Lyu, Y. Ma, M. Maggiora, S. P. Maharana, R. Maiti, S. Maity, G. Mancinelli, R. Manfredi, E. Manoni, M. Mantovano, D. Marcantonio, S. Marcello, C. Marinas, L. Martel, C. Martellini, A. Martini, T. Martinov, L. Massaccesi, M. Masuda, T. Matsuda, K. Matsuoka, D. Matvienko, S. K. Maurya, J. A. McKenna, R. Mehta, F. Meier, M. Merola, F. Metzner, M. Milesi, C. Miller, M. Mirra, K. Miyabayashi, R. Mizuk, G. B. Mohanty, N. Molina-Gonzalez, S. Mondal, S. Moneta, H.-G. Moser, M. Mrvar, R. Mussa, I. Nakamura, M. Nakao, Y. Nakazawa, A. Narimani Charan, M. Naruki, Z. Natkaniec, A. Natochii, L. Nayak, M. Nayak, G. Nazaryan, C. Niebuhr, N. K. Nisar, S. Nishida, S. Ogawa, H. Ono, Y. Onuki, P. Oskin, F. Otani, P. Pakhlov, G. Pakhlova, A. Paladino, A. Panta, E. Paoloni, S. Pardi, K. Parham, H. Park, S.-H. Park, B. Paschen, A. Passeri, S. Patra, S. Paul, T. K. Pedlar, I. Peruzzi, R. Peschke, R. Pestotnik, F. Pham, M. Piccolo, L. E. Piilonen, P. L. M. Podesta-Lerma, T. Podobnik, S. Pokharel, L. Polat, C. Praz, S. Prell, E. Prencipe, M. T. Prim, H. Purwar, N. Rad, P. Rados, G. Raeuber, S. Raiz, M. Reif, S. Reiter, M. Remnev, I. Ripp-Baudot, G. Rizzo, L. B. Rizzuto, S. H. Robertson, M. Roehrken, J. M. Roney, A. Rostomyan, N. Rout, G. Russo, D. A. Sanders, S. Sandilya, A. Sangal, L. Santelj, Y. Sato, V. Savinov, B. Scavino, C. Schmitt, M. Schnepf, C. Schwanda, A. J. Schwartz, Y. Seino, A. Selce, K. Senyo, J. Serrano, M. E. Sevior, C. Sfienti, W. Shan, C. Sharma, X. D. Shi, T. Shillington, J.-G. Shiu, D. Shtol, B. Shwartz, A. Sibidanov, F. Simon, J. B. Singh, J. Skorupa, R. J. Sobie, M. Sobotzik, A. Soffer, A. Sokolov, E. Solovieva, S. Spataro, B. Spruck, M. Starič, P. Stavroulakis, S. Stefkova, Z. S. Stottler, R. Stroili, J. Strube, M. Sumihama, K. Sumisawa, W. Sutcliffe, H. Svidras, M. Takahashi, M. Takizawa, U. Tamponi, S. Tanaka, K. Tanida, H. Tanigawa, F. Tenchini, A. Thaller, O. Tittel, R. Tiwary, D. Tonelli, E. Torassa, N. Toutounji, K. Trabelsi, I. Tsaklidis, M. Uchida, I. Ueda, Y. Uematsu, T. Uglov, K. Unger, Y. Unno, K. Uno, S. Uno, P. Urquijo, Y. Ushiroda, S. E. Vahsen, R. van Tonder, G. S. Varner, K. E. Varvell, M. Veronesi, A. Vinokurova, V. S. Vismaya, L. Vitale, V. Vobbilisetti, R. Volpe, B. Wach, M. Wakai, H. M. Wakeling, S. Wallner, E. Wang, M.-Z. Wang, Z. Wang, A. Warburton, M. Watanabe, S. Watanuki,

M. Welsch, C. Wessel, E. Won, X. P. Xu, B. D. Yabsley, S. Yamada, W. Yan, S. B. Yang, J. H. Yin, K. Yoshihara, C. Z. Yuan, Y. Yusa, L. Zani, Y. Zhang, V. Zhilich, J. S. Zhou, Q. D. Zhou, and V. I. Zhukova

(Belle II Collaboration)

(Received 6 July 2023; accepted 15 September 2023; published 17 October 2023)

We present a measurement of time-dependent rate asymmetries in $B^0 \to \phi K_S^0$ decays to search for non-standard-model physics in $b \to q\bar{q}s$ transitions. The data sample is collected with the Belle II detector at the SuperKEKB asymmetric-energy e^+e^- collider in 2019–2022 and contains $(387 \pm 6) \times 10^6$ bottom-antibottom mesons from $\Upsilon(4S)$ resonance decays. We reconstruct 162 ± 17 signal events and extract the charge-parity (CP) violating parameters from a fit to the distribution of the proper-decay-time difference of the two B mesons. The measured direct and mixing-induced CP asymmetries are $C = -0.31 \pm 0.20 \pm 0.05$ and $S = 0.54 \pm 0.26^{+0.06}_{-0.08}$, respectively, where the first uncertainties are statistical and the second are systematic. The results are compatible with the CP asymmetries observed in $b \to c\bar{c}s$ transitions.

DOI: 10.1103/PhysRevD.108.072012

I. INTRODUCTION

Measurements of CP asymmetries in loop-suppressed B meson decays are sensitive probes of physics beyond the standard model (SM). In particular, gluonic-penguin $b \to q\bar{q}s$ modes, such as $B^0 \to \phi K_S^0$, are sensitive to interfering non-SM amplitudes that carry additional weak-interaction phases. The SM reference is the mixing-induced CP asymmetry $S \equiv \sin 2\phi_1$ observed in tree-level $b \to c\bar{c}s$ transitions, where ϕ_1 (or β) equals $\arg(-V_{cd}V_{cb}^*/V_{td}V_{tb}^*)$ and V_{ij} are Cabibbo-Kobayashi-Maskawa (CKM) quark-mixing matrix elements [1,2]. The deviation from the value of S observed in $b \to c\bar{c}s$ transitions, $S = 0.699 \pm 0.017$ [3], is the key observable. For $B^0 \to \phi K_S^0$ decays, such a deviation is at most 0.02 ± 0.01 within the SM while the direct CP asymmetry C is expected to be zero [4]. The current world-average values for $B^0 \to \phi K_S^0$ are $S = 0.74^{+0.11}_{-0.13}$ and $C = 0.01 \pm 0.14$ [3]. Therefore, experimental knowledge must be improved. We present a measurement of S and C in the sample of electron-positron collisions collected by the Belle II experiment in 2019–2022 [5].

At B -factories, $B\bar{B}$ events are produced from the decay of an $\Upsilon(4S)$ resonance, where B indicates a B^+ or B^0 meson. We denote pairs of neutral B mesons as $B_{CP}B_{\rm tag}$, where B_{CP} decays into a CP -eigenstate at time t_{CP}, and $B_{\rm tag}$ decays into a flavor-specific final state at time $t_{\rm tag}$. For quantum-correlated B -meson pairs, the flavor of B_{CP} is opposite to that of $B_{\rm tag}$ at the instant when the $B_{\rm tag}$ decays. The probability to observe a $B_{\rm tag}$ meson with flavor q ($q = +1$ for B^0 and $q = -1$ for $\bar{B}^0$) and a proper-time difference $\Delta t \equiv t_{CP} - t_{\rm tag}$ between the B_{CP} and $B_{\rm tag}$ decays is

$$\mathcal{P}(\Delta t, q) = \frac{e^{-|\Delta t|/\tau_{B^0}}}{4\tau_{B^0}}\{1 + q[S\sin(\Delta m_d \Delta t) - C\cos(\Delta m_d \Delta t)]\}, \tag{1}$$

where τ_{B^0} and Δm_d are the B^0 lifetime and $B^0 - \bar{B}^0$ mixing frequency, respectively [6].

We reconstruct $B^0 \to \phi K_S^0$ decays in a sample of energy-asymmetric e^+e^- collisions at the $\Upsilon(4S)$ resonance provided by SuperKEKB and collected with the Belle II detector. The sample corresponds to (362 ± 2) fb^{-1} and contains $(387 \pm 6) \times 10^6$ $B\bar{B}$ events. We fully reconstruct B_{CP} in the ϕK_S^0 final state using the intermediate decays $\phi \to K^+K^-$ and $K_S^0 \to \pi^+\pi^-$, while we only determine the position of the $B_{\rm tag}$ decay. The flavor of the $B_{\rm tag}$ meson is inferred from the properties of all charged particles in the event not belonging to B_{CP} [7]. In order to extract the CP asymmetries, we model the distributions of signal B_{CP} and backgrounds in Δt and other discriminating variables, and then perform a likelihood fit. The last measurements, by the Belle and *BABAR* experiments, used time-dependent Dalitz-plot analyses [8,9]. This method models the interferences among the intermediate resonant and nonresonant amplitudes contributing to $B^0 \to K^+K^-K_S^0$ decays, thereby providing the best sensitivity on ϕ_1. Due to the small dataset size, which may induce multiple solutions in the Dalitz-plot approach, we perform a quasi-two-body analysis by restricting the sample to candidates reconstructed in a narrow region around the ϕ mass. This strategy offers the advantage of a simpler analysis, albeit with a reduced statistical sensitivity. We use the knowledge from the previous Dalitz-plot analyses to estimate the effect of neglecting the interferences. We test our analysis on the CP -conserving $B^+ \to \phi K^+$ decay, which has similar backgrounds and vertex resolution. Charge-conjugated modes are included throughout the paper.

II. EXPERIMENTAL SETUP

The Belle II detector [10] operates at the SuperKEKB accelerator at KEK, which collides 7 GeV electrons with 4 GeV positrons. The detector is designed to reconstruct the decays of heavy-flavor mesons and τ leptons. It consists of several subsystems arranged cylindrically around the interaction point (IP). The innermost part of the detector is equipped with a two-layer silicon-pixel detector (PXD), surrounded by a four-layer double-sided silicon-strip detector (SVD) [11]. Together, they provide information about charged-particle trajectories (tracks) and decay-vertex positions. Of the outer PXD layer, only one-sixth is installed for the data used in this work. The momenta and electric charges of charged particles are determined with a 56-layer central drift-chamber (CDC). Charged-hadron identification (PID) is provided by a time-of-propagation counter and an aerogel ring-imaging Cherenkov counter, located in the central and forward regions outside the CDC, respectively. The CDC provides additional PID information through the measurement of specific ionization. Photons are identified and electrons are reconstructed by an electromagnetic calorimeter made of CsI(Tl) crystals, covering the region outside of the PID detectors. The tracking and PID subsystems, and the calorimeter, are surrounded by a superconducting solenoid, providing an axial magnetic field of 1.5 T. The central axis of the solenoid defines the z axis of the laboratory frame, pointing approximately in the direction of the electron beam. Outside of the magnet lies the muon and K_L^0 identification system, which consists of iron plates interspersed with resistive-plate chambers and plastic scintillators.

We use simulated events to model signal and background distributions, study the detector response, and test the analysis. Quark-antiquark pairs from e^+e^- collisions, and hadron decays, are simulated using KKMC [12] with PYTHIA8 [13], and EvtGen [14], respectively. The detector response and K_S^0 decays are simulated using Geant4 [15]. Collision data and simulated samples are processed using the Belle II analysis software [16,17].

III. EVENT RECONSTRUCTION

Events containing a $B\bar{B}$ pair are selected online by a trigger based on the track multiplicity and total energy deposited in the calorimeter. We reconstruct $B^0 \to \phi K_S^0$ decays using $\phi \to K^+K^-$ and $K_S^0 \to \pi^+\pi^-$ decays, in which the four tracks are reconstructed using information from the PXD, SVD, and CDC [18]. All tracks are required to have polar angle θ within the CDC acceptance ($17° < \theta < 150°$). Tracks used to form ϕ candidates are required to have a distance of closest approach to the IP less than 2.0 cm along the z axis and less than 0.5 cm in the transverse plane to reduce contamination of tracks not generated in the collision.

Kaon and pion mass hypotheses are assigned to tracks based on information provided by the PID subsystems. The ϕ candidates are formed by combining K^+K^- pairs consistent with originating from the IP and having invariant mass within $[0.99, 1.09]$ GeV$/c^2$, where the average ϕ mass resolution is approximately 3 MeV$/c^2$. The K_S^0 candidates are formed by combining two oppositely charged particles, assumed to be pions, and requiring their invariant mass to be within $[0.480, 0.515]$ GeV$/c^2$, where the average K_S^0 mass resolution is approximately 2 MeV$/c^2$. In order to suppress combinatorial background from misreconstructed K_S^0, we require K_S^0 candidates to have a displacement of at least 0.05 cm from the ϕ decay vertex, where the average K_S^0 flight distance is 10 cm.

The beam-energy constrained mass M_{bc} and energy difference ΔE are computed for each $B^0 \to \phi K_S^0$ candidate as $M_{\mathrm{bc}} \equiv \sqrt{(E^*_{\mathrm{beam}}/c^2)^2 - (|p^*_B|/c)^2}$ and $\Delta E \equiv E^*_B - E^*_{\mathrm{beam}}$, where E^*_{beam} is the beam energy, and E^*_B and p^*_B are the energy and momentum of the B_{CP} candidate, respectively, all calculated in the center-of-mass (c.m.) frame. Signal B_{CP} candidates peak at the known B^0 mass [6] and zero in M_{bc} and ΔE, respectively, while continuum is distributed more uniformly. Only candidates satisfying $M_{\mathrm{bc}} > 5.2$ GeV$/c^2$ and $|\Delta E| < 0.2$ GeV are retained for further analysis.

The $B^0 \to \phi K_S^0$ decay vertex is determined using the `TreeFitter` algorithm [19,20]. In addition, the B_{CP} candidate is constrained to point back to the IP. The B_{tag} decay vertex is reconstructed using the remaining tracks in the event. Each track is required to have at least one measurement point in the SVD and CDC subdetectors and correspond to a total momentum greater than 50 MeV$/c$. The B_{tag} decay-vertex position is fitted using the RAVE algorithm [21], which allows for weighting the contributions from tracks that are displaced from the B_{tag} decay vertex, and thereby suppressing biases from secondary charm decays. The decay-vertex position is determined by constraining the B_{tag} direction, as determined from its decay vertex and the IP, to be collinear with its momentum vector [22].

We estimate the proper-time difference using the longitudinal decay-vertex positions, ℓ_{CP} and ℓ_{tag}, of the B_{CP} and B_{tag} mesons, respectively, as

$$\Delta t \approx \frac{\ell_{CP} - \ell_{\mathrm{tag}}}{\beta\gamma\gamma^* c}, \qquad (2)$$

where $\beta\gamma = 0.28$ is the $\Upsilon(4S)$ Lorentz boost and $\gamma^* = 1.002$ is the Lorentz factor of the B mesons in the c.m. frame. The average distance between the B_{CP} and B_{tag} vertices is approximately 100 μm along the z axis. The B -decay vertex resolution along the z axis is approximately 35 μm for simulated $B^0 \to \phi K_S^0$ decays. We apply loose χ^2 probability requirements to both the B_{CP} and B_{tag} vertices. Events having a Δt uncertainty $\sigma_{\Delta t}$ greater than 2.0 ps, where the average value is approximately 0.5 ps, are not included in the analysis, as they constitute less than 2% of the signal events and do not contribute to the determination of S.

The dominant sources of background come from continuum $e^+e^- \to q\bar{q}$ events, where q indicates a u, d, c, or s quark. A boosted-decision-tree (BDT) classifier is trained on simulated samples to combine several topological variables that provide separation between continuum and signal events [23]. The variables included in the BDT are the following, in order of decreasing discriminating power: the cosine of the angle between the thrust axes of B_{CP} and B_{tag} [24], the modified Fox-Wolfram moments introduced in Ref. [25], the thrust of B_{tag} [26,27], the ratio of the zeroth to the first Fox-Wolfram moment [28], and the harmonic moments calculated with respect to the thrust axis. We impose a minimum requirement on the output of the BDT, $\mathcal{O}_{\mathrm{CS}}$, that retains more than 95% of the signal, while rejecting more than 55% of the continuum events. The transformed output of the classifier, defined as $\mathcal{O}'_{\mathrm{CS}} = \log[(\mathcal{O}_{\mathrm{CS}} - \mathcal{O}_{\mathrm{CS}}^{\mathrm{min}})/(\mathcal{O}_{\mathrm{CS}}^{\mathrm{max}} - \mathcal{O}_{\mathrm{CS}})]$, where $\mathcal{O}_{\mathrm{CS}}^{\mathrm{min}}$ and $\mathcal{O}_{\mathrm{CS}}^{\mathrm{max}}$ are the minimum and maximum values of the selected events, is included in the fit. The signal and remaining background events are approximately Gaussian-distributed in this variable and are therefore simple to model.

An additional requirement $|\Delta E| < 50$ MeV further suppresses continuum and misreconstructed $B \to \phi K^*$ decays. To reduce the contamination from nonresonant $B^0 \to K^+K^-K_S^0$ decays and other modes leading to the same final state, events are required to satisfy $|m(K^+K^-) - m_\phi| <$ 10 MeV$/c^2$, where m_ϕ is the known ϕ meson mass [6].

The same event reconstruction is applied on $B^+ \to \phi K^+$ decays, except for the K_S^0 selection, which is replaced by a K^+ track with a stringent PID requirement. This is more than 90% efficient on the signal, while rejecting around 30% of misidentified charged particles. We achieve a total signal reconstruction efficiency of 33% for $B^0 \to \phi K_S^0$ and 40% for $B^+ \to \phi K^+$.

Events with multiple candidates account for approximately 6% of the data. We keep the candidate with the highest B_{CP} vertex χ^2 probability. The criterion retains the correct signal candidate 67% of the times using simulated events. We check that the candidate selection does not bias the Δt distribution by comparing the results of lifetime fits to the B^0 and B^+ samples with known values [6].

IV. TIME-DEPENDENT *CP*-ASYMMETRY FIT

The distributions of signal and backgrounds are described in a likelihood fit to extract the CP asymmetries. We consider the following contributions to the sample composition: signal $B^0 \to \phi K_S^0$ events, nonresonant $B^0 \to K^+K^-K_S^0$ background, and continuum background. Additional $B\bar{B}$ background events are treated as a source of systematic uncertainty, as they are estimated to be at most 2% of the signal yield, according to simulation. Low-multiplicity events contribute at less than the level of the $B\bar{B}$ backgrounds in the simulation, and are distributed like continuum in the variables used in the fit, so they are treated as part of the continuum background. We model the distributions of signal and background events in the M_{bc}, $\mathcal{O}'_{\mathrm{CS}}$, $\cos\theta_H$, and Δt variables. The M_{bc} and $\mathcal{O}'_{\mathrm{CS}}$ variables provide discrimination between signal and continuum background. The helicity angle θ_H, defined as the angle between the momentum of the B^0 and that of the positively charged kaon in the ϕ rest frame, is used to distinguish between signal and nonresonant components. The Δt variable and tag-flavor q provide access to the time-dependent CP asymmetries. In addition, we use $\sigma_{\Delta t}$ as a conditional observable to model the per-event resolution.

We extract the CP asymmetries using an extended maximum-likelihood fit to the unbinned distributions of the discriminating variables. The total probability density function (PDF) is given by the product of the four one-dimensional PDFs, since the dependences among the fit observables are negligible. We model the M_{bc} distribution using an ARGUS function [29] for continuum and a Gaussian function with shared parameters for the $B^0 \to \phi K_S^0$ and $B^0 \to K^+K^-K_S^0$ components. The continuum shape is fixed from a fit to the $|\Delta E| > 0.1$ GeV sideband, while the signal-shape parameters are determined by the fit. We check that the continuum shapes are not biased by $B^0 \to \phi K^{*0}$, $B^+ \to \phi K^{*+}$, and other B^0 and B^+ decay modes, contributing in total to less than 1% of the events in the ΔE sideband. The $\mathcal{O}'_{\mathrm{CS}}$ distribution is modeled using the sum of two Gaussian functions with a common mean and constrained proportions for continuum, and a Gaussian function with asymmetric widths and shared parameters for the $B^0 \to \phi K_S^0$ and $B^0 \to K^+K^-K_S^0$ components. The $\mathcal{O}'_{\mathrm{CS}}$ shape-parameters are determined from events in the ΔE sideband for continuum, and using simulated events for signal. The $\cos\theta_H$ distribution of continuum is modeled with a second-order polynomial determined from ΔE sideband events. We verify using simulated samples that the $B^0 \to \phi K_S^0$ and $B^0 \to K^+K^-K_S^0$ components follow a $\cos^2\theta_H$ and a uniform distribution, respectively, as expected from angular momentum conservation, and the detector acceptance does not affect their shapes.

The B_{tag} flavor is identified using a category-based B -flavor tagging algorithm from the particles in the event that are not associated with the B_{CP} candidate [7]. The tagging algorithm provides for each B_{tag} candidate a flavor (q) and the tag-quality $r = 1$–$2w$. The latter is a function of the wrong-tag probability w and ranges from $r = 0$ for no discrimination power to $r = 1$ for unambiguous flavor assignment. Taking into account the effect of imperfect flavor assignment, Eq. (1) becomes

$$\mathcal{P}(\Delta t, q) = \frac{e^{-|\Delta t|/\tau_{B^0}}}{4\tau_{B^0}} \Big\{ 1 - q\Delta w + q a_\epsilon^{\mathrm{tag}}(1-2w) + [q(1-2w) + a_\epsilon^{\mathrm{tag}}(1-q\Delta w)] \times [S\sin(\Delta m_d \Delta t) - C\cos(\Delta m_d \Delta t)] \Big\}, \tag{3}$$

where Δw is the wrong-tag probability difference between events tagged as B^0 and $\bar{B}^0$, and $a_\epsilon^{\mathrm{tag}}$ is the tagging-efficiency-asymmetry between B^0 and $\bar{B}^0$.

The effect of finite Δt resolution is taken into account by modifying Eq. (3) as follows:

$$\mathcal{F}(\Delta t, q|\sigma_{\Delta t}) = \int \mathcal{P}(\Delta t', q)\mathcal{R}(\Delta t - \Delta t'|\sigma_{\Delta t}) d\Delta t', \tag{4}$$

where $\mathcal{R}$ is the resolution function, conditional on the per-event Δt uncertainty $\sigma_{\Delta t}$. Its parametrization, as determined in $B^0 \to D^{(*)-}\pi^+$ decays [30], consists of the sum of three components,

$$\begin{aligned}\mathcal{R}(\delta t|\sigma_{\Delta t}) = {} & (1 - f_t - f_{\mathrm{OL}})G(\delta t|m_G\sigma_{\Delta t}, s_G\sigma_{\Delta t}) \\ & + f_t(\sigma_{\Delta t})R_t(\delta t|m_t\sigma_{\Delta t}, s_t\sigma_{\Delta t}, k/\sigma_{\Delta t}, f_>, f_<) \\ & + f_{\mathrm{OL}}G(\delta t|0, \sigma_0),\end{aligned} \tag{5}$$

where δt is the difference between the observed and the true Δt. The first component is described by a Gaussian function with mean m_G and width s_G scaled by $\sigma_{\Delta t}$, which accounts for the core of the distribution. The second component R_t is the sum of a Gaussian function and the convolution of a Gaussian with two oppositely sided exponential functions,

$$\begin{aligned}R_t(x|\mu, \sigma, k, f_>, f_<) = {} & (1 - f_< - f_>)G(x|\mu, \sigma) \\ & + f_< G(x|\mu, \sigma) \otimes k\exp_<(kx) \\ & + f_> G(x|\mu, \sigma) \otimes k\exp_>(-kx),\end{aligned} \tag{6}$$

where $\exp_>(kx) = \exp(kx)$ if $x > 0$ or zero otherwise, and similarly for $\exp_<(kx)$. The exponential tails arise from intermediate displaced charm-hadron vertices from the B_{tag} decay. The fraction f_t is zero at low values of $\sigma_{\Delta t}$ and steeply reaches a plateau of 0.2 at $\sigma_{\Delta t} = 0.25$ ps. The third component, which accounts for outlier events contributing with a fraction of less than 1%, is modeled with a Gaussian function having a large width σ_0 of 200 ps. The effect on the resolution function of the small momentum of the B^0 in the $\Upsilon(4S)$ frame is taken into account as a systematic uncertainty.

We divide our sample into seven intervals (bins) of the tag-quality variable r, with boundaries (0.0, 0.1, 0.25, 0.45, 0.6, 0.725, 0.875, 1.0), to gain statistical sensitivity from events with different wrong-tag fractions. The response of the tagging algorithm and detector Δt resolution is calibrated from a simultaneous fit of w, Δw, $a_\epsilon^{\mathrm{tag}}$, and resolution-function parameters in the seven r-bins, using flavor-specific $B^0 \to D^{(*)-}\pi^+$ decays [31]. The effective flavor tagging efficiency, defined as $\sum_i \varepsilon_i(1-2w_i)^2$, where ε_i is the fraction of events associated with a tag decision and w_i is the wrong-tag probability in the ith r bin, is $(31.69 \pm 0.35)\%$, where the uncertainty is statistical. We verify in simulation the compatibility of the flavor tagging and resolution function between the calibration and signal decay modes. We use the flavor-tagging parameters obtained from $B^+ \to \bar{D}^0\pi^+$ decays to calibrate the flavor tagger and resolution function in the $B^+ \to \phi K^+$ control channel.

The Δt distribution of the continuum background is modeled using events from the ΔE sideband and allowing for an asymmetry in the yields of oppositely tagged events. A double Gaussian parametrization, with means and widths scaled by $\sigma_{\Delta t}$, describes the data accurately. The Δt distribution of the $B^0 \to K^+K^-K_S^0$ background is parametrized using the same detector response as for signal. Its CP asymmetries are fixed to the known values [3].

The nominal fits to the control and signal samples determine the continuum yields and the sum of the resonant and nonresonant yields in the seven r-bins. We also determine the fraction of the resonant yields with respect to the sum of the resonant and nonresonant yields directly in the data. In addition, the mean and width of the Gaussian function describing the resonant and nonresonant components in M_{bc} and the asymmetry in the normalization of oppositely tagged continuum-background events are determined by the fit. Finally, the fit determines the CP asymmetries, for a total of 20 free parameters.

The fit results are reported in Table I. In the control sample, we find 581 ± 33 signal $B^+ \to \phi K^+$, 70 ± 23 nonresonant, and 5730 ± 77 continuum events. The relevant data distributions are displayed in Fig. 1, with fit projections overlaid, under selections in the analysis variables that enhance the signal component.

TABLE I. Results of the fit to the signal and control samples.

	$B^0 \to \phi K_S^0$	$B^+ \to \phi K^+$
Resonant yield	162 ± 17	581 ± 33
Nonresonant yield	21 ± 12	70 ± 23
Continuum yield	1169 ± 35	5730 ± 77
C	-0.31 ± 0.20	-0.12 ± 0.10
S	0.54 ± 0.26	-0.09 ± 0.12

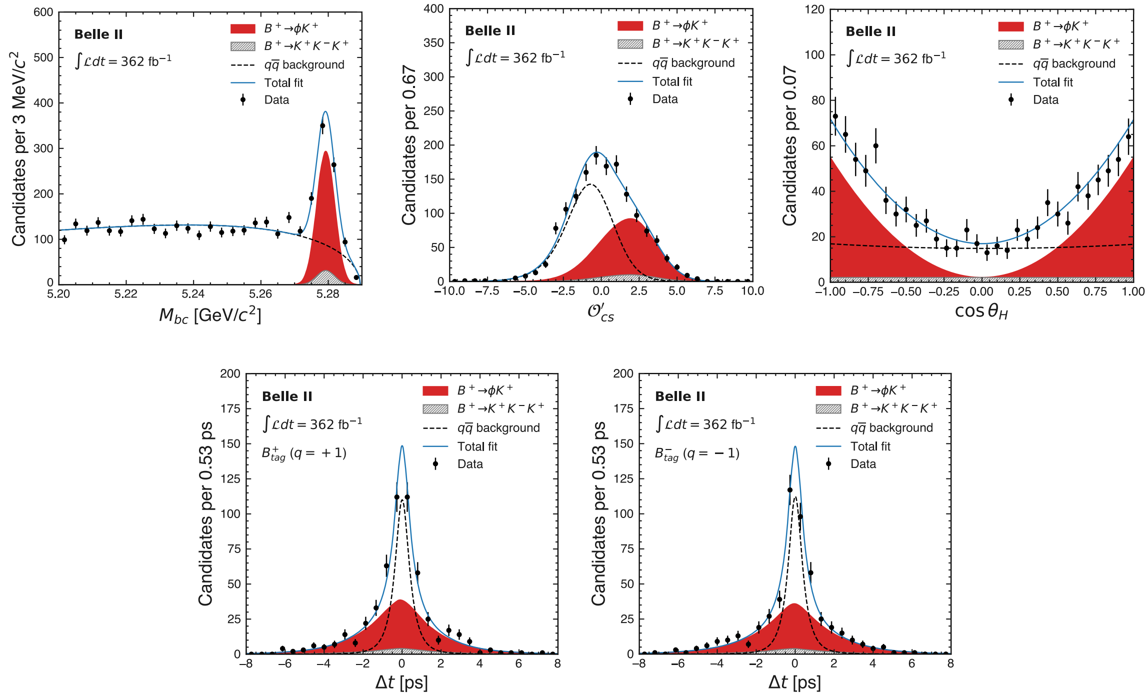

FIG. 1. Distributions of (top left) M_{bc}, (top center) $\mathcal{O}'_{\mathrm{CS}}$, (top right) $\cos\theta_H$, (bottom left) Δt for B^+ -tagged and (bottom right) Δt for B^- -tagged $B^+ \to \phi K^+$ candidates (data points) with fits overlaid (curves and stacked shaded areas). The M_{bc} distribution is displayed for candidates with $\mathcal{O}'_{\mathrm{CS}} > -1$ and the $\mathcal{O}'_{\mathrm{CS}}$ distribution is displayed for candidates with $M_{\mathrm{bc}} > 5.27\ \mathrm{GeV}/c^2$. The $\cos\theta_H$ and Δt distributions are displayed for candidates with $\mathcal{O}'_{\mathrm{CS}} > -1$ and $M_{\mathrm{bc}} > 5.27\ \mathrm{GeV}/c^2$.

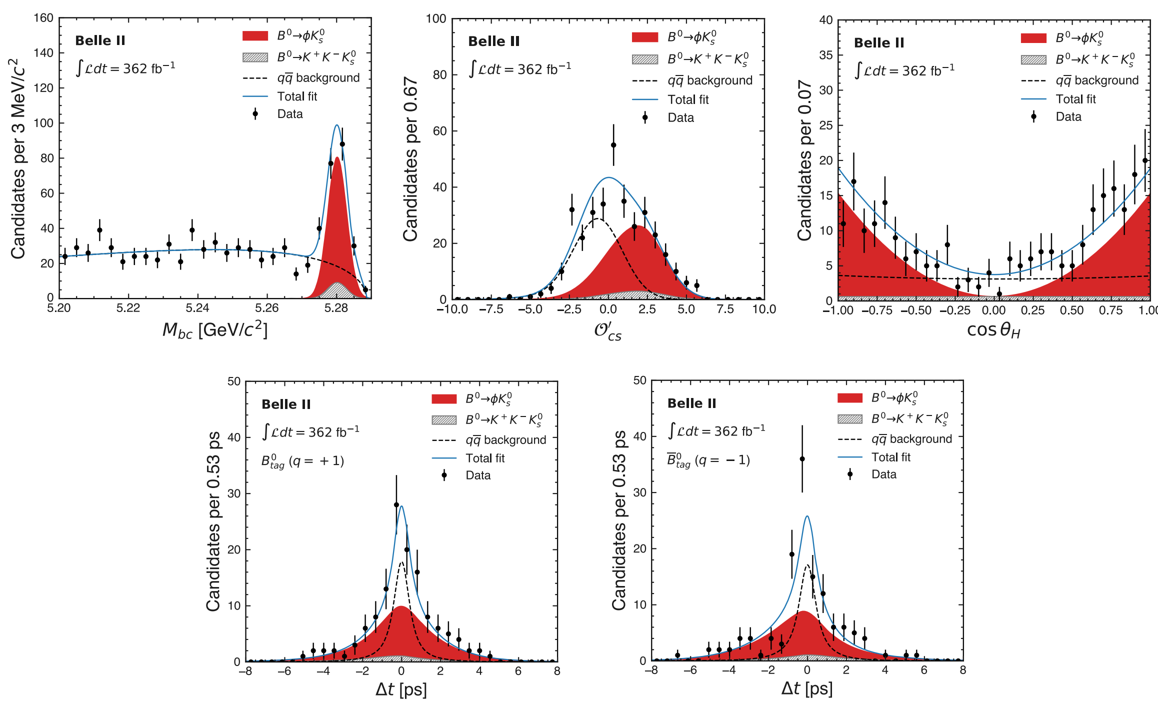

FIG. 2. Distributions of (top left) M_{bc}, (top center) $\mathcal{O}'_{\mathrm{CS}}$, (top right) $\cos\theta_H$, (bottom left) Δt for B^0 -tagged and (bottom right) Δt for $\bar{B}^0$ -tagged $B^0 \to \phi K^0_S$ candidates (data points) with fits overlaid (curves and stacked shaded areas). The M_{bc} distribution is displayed for candidates with $\mathcal{O}'_{\mathrm{CS}} > -1$ and the $\mathcal{O}'_{\mathrm{CS}}$ distribution is displayed for candidates with $M_{\mathrm{bc}} > 5.27\ \mathrm{GeV}/c^2$. The $\cos\theta_H$ and Δt distributions are displayed for candidates with $\mathcal{O}'_{\mathrm{CS}} > -1$ and $M_{\mathrm{bc}} > 5.27\ \mathrm{GeV}/c^2$.

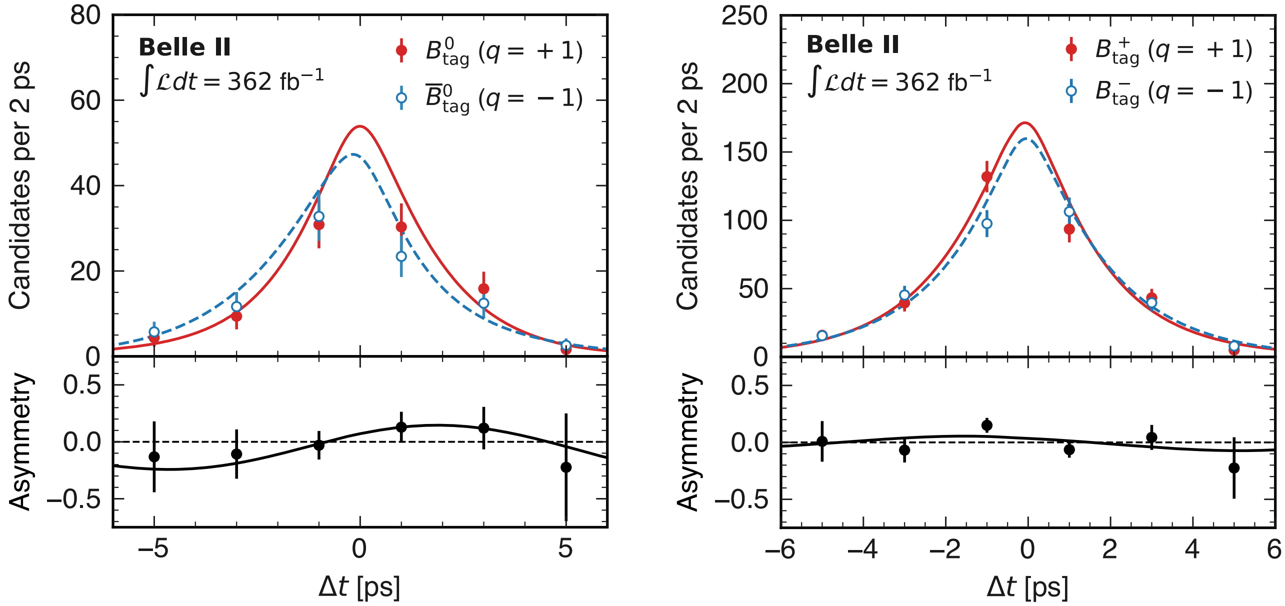

FIG. 3. Distributions, and fit projections, of Δt for flavor-tagged (left) $B^0 \to \phi K^0_S$ and (right) $B^+ \to \phi K^+$ candidates subtracted of the continuum background. The fit PDFs corresponding to $q = -1$ and $q = +1$ tagged distributions are shown as dashed and solid curves, respectively. The yield asymmetries, defined as $(N(q = +1) - N(q = -1))/(N(q = +1) + N(q = -1))$, are displayed in the bottom subpanels.

The control-sample CP asymmetries are $C = -0.12 \pm 0.10$ and $S = -0.09 \pm 0.12$, where the uncertainties are statistical only, with correlation coefficient $\rho = 0.06$. The results are compatible with the null asymmetries we expect. In the fit to the signal $B^0 \to \phi K^0_S$ sample, displayed under the same signal-enhancing selections in Fig. 2, we find 162 ± 17 signal, 21 ± 12 nonresonant, and 1169 ± 35 continuum events. The corresponding CP asymmetries are $C = -0.31 \pm 0.20$ and $S = 0.54 \pm 0.26$, where the uncertainties are statistical only, with correlation coefficient $\rho = 0.01$. The observed continuum background asymmetry is compatible with zero. The Δt distributions for tagged signal decays, after subtracting the continuum background [32], are displayed in Fig. 3, along with the resulting CP-violating asymmetries.

V. SYSTEMATIC UNCERTAINTIES

Contributions from all considered sources of systematic uncertainty are listed in Table II. We consider uncertainties associated with the calibration of the flavor tagging and resolution function, fit model, and determination of Δt.

The leading contribution to the total systematic uncertainty on C arises by neglecting a possible time-integrated CP asymmetry from $B\bar{B}$ backgrounds. The main systematic uncertainty on S comes from the fit bias, due to the modest statistical precision to which the fraction of $B^0 \to K^+K^-K^0_S$ backgrounds can be determined with the current sample size.

A. Calibration with $B^0 \to D^{(*)-}\pi^+$ decays

We assess the uncertainty associated with the resolution function and flavor tagging parameters using simplified simulated samples. We generate ensembles assuming for each an alternative value for the above parameters sampled

TABLE II. Summary of systematic uncertainties.

Source	$\sigma(C)$	$\sigma(S)$
Calibration with $B^0 \to D^{(*)-}\pi^+$ decays		
Calibration sample size	± 0.010	± 0.009
Calibration sample systematic	± 0.010	± 0.012
Sample dependence	$+0.005$	$+0.021$
Fit model		
Fit bias	${}^{+0.028}_{-0.017}$	${}^{+0.033}_{-0.062}$
$B^0 \to K^+K^-K^0_S$ backgrounds	$+0.020$	-0.011
Fixed fit shapes	± 0.009	± 0.022
τ_{B^0} and Δm_d	± 0.006	± 0.022
$C_{K^+K^-K^0_S}$ and $S_{K^+K^-K^0_S}$	± 0.014	± 0.013
$B\bar{B}$ background asymmetry	${}^{+0.019}_{-0.030}$	${}^{+0.017}_{-0.031}$
Tag-side interference	<0.001	$+0.012$
Candidate selection	-0.032	-0.002
Δt measurement		
Tracker misalignment	-0.002	-0.002
Momentum scale	± 0.001	± 0.001
Beam spot	± 0.002	± 0.002
Δt approximation	<0.001	-0.018
Total systematic	${}^{+0.046}_{-0.052}$	${}^{+0.058}_{-0.082}$
Statistical	± 0.201	± 0.256

from the statistical covariance matrix determined in the $B^0 \to D^{(*)-}\pi^+$ control sample. Each ensemble is fitted using the nominal values of the calibration parameters and the standard deviation of the observed biases is used as a systematic uncertainty.

A similar procedure is used to assess a systematic uncertainty due to the systematic uncertainties on the calibration parameters, in which the ensembles are generated by varying each parameter independently within their systematic uncertainty.

We estimate the impact of differences in the resolution function and tagging performance between the signal and calibration samples. We apply the resolution function and flavor-tagging calibration obtained from a simulated $B^0 \to D^{(*)-}\pi^+$ sample and repeat the measurement of C and S over an ensemble of simulated $B^0 \to \phi K_S^0$ events. The average deviation of the CP asymmetries from their generated values is assigned as a systematic uncertainty.

B. Fit model

To validate how accurately the fit determines the underlying physics parameters in the presence of backgrounds, we generate ensemble datasets that contain all the fit components. For each ensemble, we sample alternative values of C and S within the physical boundaries, and the fraction of the resonant events over the sum of resonant and nonresonant decays between 0.7 and 1.0, to account for the statistical precision on the observed value $f_{\phi K} = 0.89 \pm 0.07$. Due to the limited sample size, we assign a conservative systematic uncertainty for the fit bias by taking the largest deviations of the fitted values of C and S from their generated values. We also check that the relative magnitude of this systematic uncertainty with respect to the statistical uncertainty remains constant for larger sample sizes.

We study the effect of neglecting interference between the signal and nonresonant backgrounds using simulated samples, where the $B^0 \to \phi K_S^0$ and $B^0 \to K^+K^-K_S^0$ components are generated coherently using a complete Dalitz-plot description of the decay [8]. We apply the nominal fit to these samples, where the nonresonant yields are determined by the fit and the CP -asymmetries of the backgrounds, $C_{K^+K^-K_S^0}$ and $S_{K^+K^-K_S^0}$, are fixed to their generated values, neglecting interference with the signal. The difference between the generated and fitted values of the CP -asymmetries of the signal is assigned as a systematic uncertainty.

The effect of fixing the PDF shapes of the $M_{\rm bc}$, $\mathcal{O}'_{\rm CS}$, $\cos\theta_H$, and Δt distributions in continuum, and $\mathcal{O}'_{\rm CS}$ distribution in signal and nonresonant background, is estimated from ensemble datasets. We generate simulated datasets by varying the shape parameters, in order to cover for the empirical parametrization and statistical uncertainty, and fix them to their nominal values in the fit. The resulting standard deviation on the distributions of C and S is used to estimate the corresponding systematic uncertainty.

The same procedure is applied to estimate the systematic uncertainty associated with the external inputs used for the lifetime $\tau_{B^0} = (1.519 \pm 0.004)$ ps, mixing frequency $\Delta m_d = (0.507 \pm 0.002)$ ps^{-1}, and CP asymmetries $C = 0.06 \pm 0.08$ and $S = -0.68^{+0.09}_{-0.10}$ of the nonresonant background.

Simulation shows that the residual $B\bar{B}$ backgrounds is at most 2% of the signal yield. We generate ensemble datasets containing an additional $B\bar{B}$ background component with PDF shapes modeled after the $B^0 \to \phi K_S^0$ or $B^0 \to K^+K^-K_S^0$ distributions and by conservatively varying the $B\bar{B}$ background CP asymmetries between $+1$ and -1. The $B\bar{B}$ backgrounds are neglected in the fit to these datasets. The corresponding systematic uncertainty is obtained by taking the largest deviations of C and S from their generated values.

The time evolution given in Eq. (1) assumes that the $B_{\rm tag}$ decays in a flavor-specific final state. We study the impact of the tag-side interference, i.e., neglecting the effect of CKM-suppressed $b \to u\bar{c}d$ decays in the $B_{\rm tag}$ in the model for Δt [33]. The observed asymmetries can be corrected for this effect by using the knowledge from previous measurements [3]. We conservatively assume all events to be tagged by hadronic B decays, for which the effect is largest, and take the difference with respect to the observed asymmetries as a systematic uncertainty.

The effect of multiple candidates is evaluated by repeating the analysis with all the candidates and taking the difference with respect to the nominal candidate selection as a systematic uncertainty.

C. Δt measurement

The impact of the detector misalignment is tested on simulated samples reconstructed with various misalignment configurations.

The uncertainty on the momentum scale of charged particles due to the imperfect modeling of the magnetic field has a small impact on the CP asymmetries [31].

Similarly, the uncertainty on the coordinates of the e^+e^- interaction region (beam spot) has a subleading effect [31].

We do not account for the angular distribution of the B meson pairs in the c.m. frame when calculating Δt using Eq. (2). Therefore, we estimate the effect of the Δt approximation on simulated samples, where the generated and reconstructed time differences can be compared.

VI. SUMMARY

A measurement of CP violation in $B^0 \to \phi K_S^0$ decays is presented using data from the Belle II experiment. We find 162 ± 17 signal candidates in a sample containing $(387 \pm 6) \times 10^6$ $B\bar{B}$ events. The values of the CP asymmetries are

$$C = -0.31 \pm 0.20 \pm 0.05 \quad \text{and} \quad S = 0.54 \pm 0.26^{+0.06}_{-0.08},$$

where the first uncertainty is statistical, and the second is systematic. The results are compatible with previous determinations from Belle and *BABAR* [8,9] and have a similar uncertainty on C, despite using a data sample 2.0 and 1.2 times smaller, respectively. When compared to measurements using a similar quasi-two-body approach [34,35], there is a 10% to 20% improvement on the statistical uncertainty on S for the same number of signal events. No significant discrepancy in the CP asymmetries between $b \to q\bar{q}s$ and $b \to c\bar{c}s$ transitions is observed.

ACKNOWLEDGMENTS

This work, based on data collected using the Belle II detector, which was built and commissioned prior to March 2019, was supported by Science Committee of the Republic of Armenia Grant No. 20TTCG-1C010; Australian Research Council and Research Grants No. DP200101792, No. DP210101900, No. DP210102831, No. DE220100462, No. LE210100098, and No. LE230100085; Austrian Federal Ministry of Education, Science and Research, Austrian Science Fund No. P31361-N36 and No. J4625-N, and Horizon 2020 ERC Starting Grant No. 947006 "InterLeptons"; Natural Sciences and Engineering Research Council of Canada, Compute Canada and CANARIE; National Key R&D Program of China under Contract No. 2022YFA1601903, National Natural Science Foundation of China and Research Grants No. 11575017, No. 11761141009, No. 11705209, No. 11975076, No. 12135005, No. 12150004, No. 12161141008, and No. 12175041, and Shandong Provincial Natural Science Foundation Project ZR2022JQ02; the Ministry of Education, Youth, and Sports of the Czech Republic under Contract No. LTT17020 and Charles University Grant No. SVV 260448 and the Czech Science Foundation Grant No. 22-18469S; European Research Council, Seventh Framework PIEF-GA-2013-622527, Horizon 2020 ERC-Advanced Grants No. 267104 and No. 884719, Horizon 2020 ERC-Consolidator Grant No. 819127, Horizon 2020 Marie Sklodowska-Curie Grant Agreement No. 700525 "NIOBE" and No. 101026516, and Horizon 2020 Marie Sklodowska-Curie RISE project JENNIFER2 Grant Agreement No. 822070 (European grants); L'Institut National de Physique Nucléaire et de Physique des Particules (IN2P3) du CNRS (France); BMBF, DFG, HGF, MPG, and AvH Foundation (Germany); Department of Atomic Energy under Project Identification No. RTI 4002 and Department of Science and Technology (India); Israel Science Foundation Grant No. 2476/17, U.S.-Israel Binational Science Foundation Grant No. 2016113, and Israel Ministry of Science Grant No. 3-16543; Istituto Nazionale di Fisica Nucleare and the Research Grants BELLE2; Japan Society for the Promotion of Science, Grant-in-Aid for Scientific Research Grants No. 16H03968, No. 16H03993, No. 16H06492, No. 16K05323, No. 17H01133, No. 17H05405, No. 18K03621, No. 18H03710, No. 18H05226, No. 19H00682, No. 22H00144, No. 26220706, and No. 26400255, the National Institute of Informatics, and Science Information NETwork 5 (SINET5), and the Ministry of Education, Culture, Sports, Science, and Technology (MEXT) of Japan; National Research Foundation (NRF) of Korea Grants No. 2016R1-D1A1B-02012900, No. 2018R1-A2B-3003643, No. 2018R1-A6A1A-06024970, No. 2019R1-I1A3A-01058933, No. 2021R1-A6A1A-03043957, No. 2021R1-F1A-1060423, No. 2021R1-F1A-1064008, No. 2022R1-A2C-1003993, and No. RS-2022-00197659, Radiation Science Research Institute, Foreign Large-size Research Facility Application Supporting project, the Global Science Experimental Data Hub Center of the Korea Institute of Science and Technology Information and KREONET/GLORIAD; Universiti Malaya RU grant, Akademi Sains Malaysia, and Ministry of Education Malaysia; Frontiers of Science Program Contracts No. FOINS-296, No. CB-221329, No. CB-236394, No. CB-254409, and No. CB-180023, and SEP-CINVESTAV Research Grant No. 237 (Mexico); the Polish Ministry of Science and Higher Education and the National Science Center; the Ministry of Science and Higher Education of the Russian Federation, Agreement No. 14.W03.31.0026, and the HSE University Basic Research Program, Moscow; University of Tabuk Research Grants No. S-0256-1438 and No. S-0280-1439 (Saudi Arabia); Slovenian Research Agency and Research Grants No. J1-9124 and No. P1-0135; Agencia Estatal de Investigacion, Spain Grant No. RYC2020-029875-I and Generalitat Valenciana, Spain Grant No. CIDEGENT/2018/020 Ministry of Science and Technology and Research Grants No. MOST106-2112-M-002-005-MY3 and No. MOST107-2119-M-002-035-MY3, and the Ministry of Education (Taiwan); Thailand Center of Excellence in Physics; TUBITAK ULAKBIM (Turkey); National Research Foundation of Ukraine, Project No. 2020.02/0257, and Ministry of Education and Science of Ukraine; the U.S. National Science Foundation and Research Grants No. PHY-1913789 and No. PHY-2111604, and the U.S. Department of Energy and Research Awards No. DE-AC06-76RLO1830, No. DE-SC0007983, No. DE-SC0009824, No. DE-SC0009973, No. DE-SC0010007, No. DE-SC0010073, No. DE-SC0010118, No. DE-SC0010504, No. DE-SC0011784, No. DE-SC0012704, No. DE-SC0019230, No. DE-SC0021274, No. DE-SC0022350, No. DE-SC0023470; and the Vietnam Academy of Science and Technology (VAST) under Grant No. DL0000.05/21-23. These acknowledgements are not to be interpreted as an endorsement of any statement made by any of our institutes, funding agencies, governments, or their representatives. We thank the SuperKEKB team for delivering high-luminosity collisions; the KEK cryogenics group for the efficient operation of the detector solenoid magnet; the KEK computer group and the NII for on-site computing support and SINET6 network support; and the raw-data centers at BNL, DESY, GridKa, IN2P3, INFN, and the University of Victoria for offsite computing support.

[1] N. Cabibbo, Phys. Rev. Lett. **10**, 531 (1963).
[2] M. Kobayashi and T. Maskawa, Prog. Theor. Phys. **49**, 652 (1973).
[3] Y. S. Amhis *et al.* (HFLAV Collaboration), Phys. Rev. D **107**, 052008 (2023).
[4] M. Beneke, Phys. Lett. B **620**, 143 (2005).
[5] The coefficients $(S,-C)$ are written (S, A) elsewhere.
[6] R. L. Workman *et al.* (Particle Data Group), Prog. Theor. Exp. Phys. **2022**, 083C01 (2022).
[7] F. Abudinén *et al.* (Belle II Collaboration), Eur. Phys. J. C **82**, 283 (2022).
[8] Y. Nakahama *et al.* (Belle Collaboration), Phys. Rev. D **82**, 073011 (2010).
[9] J. P. Lees *et al.* (*BABAR* Collaboration), Phys. Rev. D **85**, 112010 (2012).
[10] T. Abe *et al.* (Belle II Collaboration), arXiv:1011.0352.
[11] K. Adamczyk *et al.* (Belle II SVD Collaboration), J. Instrum. **17**, P11042 (2022).
[12] S. Jadach, B. F. L. Ward, and Z. Wąs, Comput. Phys. Commun. **130**, 260 (2000).
[13] T. Sjöstrand, R. Corke, N. Desai, P. Ilten, S. Mrenna, S. Prestel, C. O. Rasmussen, and P. Z. Skands, Comput. Phys. Commun. **191**, 159 (2015).
[14] D. J. Lange, Nucl. Instrum. Methods Phys. Res., Sect. A **462**, 152 (2001).
[15] S. Agostinelli *et al.* (GEANT4 Collaboration), Nucl. Instrum. Methods Phys. Res., Sect. A **506**, 250 (2003).
[16] T. Kuhr, C. Pulvermacher, M. Ritter, T. Hauth, and N. Braun (Belle II Framework Software Group), Comput. Software Big Sci. **3**, 1 (2019).
[17] 10.5281/zenodo.5574115.
[18] V. Bertacchi *et al.* (Belle II Tracking Group), Comput. Phys. Commun. **259**, 107610 (2021).
[19] W. D. Hulsbergen, Nucl. Instrum. Methods **552**, 566 (2005).
[20] J.-F. Krohn *et al.* (Belle II Analysis Software Group), Nucl. Instrum. Methods Phys. Res., Sect. A **976**, 164269 (2020).
[21] W. Waltenberger, W. Mitaroff, F. Moser, B. Pflugfelder, and H. V. Riedel, J. Phys. Conf. Ser. **119**, 032037 (2008).
[22] S. Dey and A. Soffer, Springer Proc. Phys. **248**, 411 (2020).
[23] T. Chen and C. Guestrin, *Proceedings of the 22nd ACM SIGKDD International Conference on Knowledge Discovery and Data Mining* (Association for Computing Machinery, New York, USA, 2016).
[24] Ed. A. J. Bevan, B. Golob, Th. Mannel, S. Prell, and B. D. Yabsley, Eur. Phys. J. C **74**, 3026 (2014).
[25] S. H. Lee *et al.* (Belle Collaboration), Phys. Rev. Lett. **91**, 261801 (2003).
[26] S. Brandt, C. Peyrou, R. Sosnowski, and A. Wroblewski, Phys. Lett. **12**, 57 (1964).
[27] E. Farhi, Phys. Rev. Lett. **39**, 1587 (1977).
[28] G. C. Fox and S. Wolfram, Phys. Rev. Lett. **41**, 1581 (1978).
[29] H. Albrecht *et al.* (ARGUS Collaboration), Phys. Lett. B **241**, 278 (1990).
[30] F. Abudinén *et al.* (Belle II Collaborataion), Phys. Rev. D **107**, L091102 (2023).
[31] I. Adachi *et al.* (Belle II Collaboration), arXiv:2302.12898.
[32] M. Pivk and F. R. Le Diberder, Nucl. Instrum. Methods Phys. Res., Sect. A **555**, 356 (2005).
[33] O. Long, M. Baak, R. N. Cahn, and D. Kirkby, Phys. Rev. D **68**, 034010 (2003).
[34] B. Aubert *et al.* (*BABAR* Collaboration), Phys. Rev. D **71**, 091102 (2005).
[35] K.-F. Chen *et al.* (Belle Collaboration), Phys. Rev. Lett. **98**, 031802 (2007).